



Full Text View

[Volume 32, Issue 6 \(June 2002\)](#)

Journal of Physical Oceanography

 Article: pp. 1947–1959 | [Abstract](#) | [PDF \(748K\)](#)

Is There a Meridional Overturning Cell in the Pacific and Indian Oceans?

Doron Nof*

Department of Oceanography, The Florida State University, Tallahassee, Florida

(Manuscript received March 5, 2001, in final form January 5, 2002)

DOI: 10.1175/1520-0485(2002)032<1947:ITAMOC>2.0.CO;2

ABSTRACT

The diagnostic quasi-island model of Nof addressing the exchange between the South Atlantic and the Southern Ocean is extended to the exchange between the Pacific–Indian Ocean system and the Southern Ocean. The new calculations suggest that, in a similar fashion to the Atlantic Ocean, the Indian and Pacific Oceans have a meridional overturning cell with a transport of $18 \pm 5 \text{ Sv}$ ($1 \text{ Sv} \equiv 10^6 \text{ m}^3 \text{ s}^{-1}$). In contrast to the Atlantic in which there is deep water formation resulting in a cell that extends all the way from the surface to the bottom, however, the Indian and Pacific circulation cell is *shallow* in the sense that it does not occupy the entire water column. As in the Atlantic case, the cell is driven by *both* winds and thermohaline processes, but the calculation does not require solving the complete wind–thermohaline problem. The computational method takes Africa, Asia, and Europe to compose a “pseudo island”; that is, the combined continent is entirely surrounded by water but has no net circulation around it. The continuation of sea level around the continent allows one to compute analytically the zonal upper-layer transport that is first forced meridionally from the Southern Ocean to the Pacific and Indian Oceans and then forced down to lower levels. Although there are no direct observations to support or refute the idea of a shallow cell in these oceans, the concept is consistent with earlier inverse calculations, with the observed distribution of silicate, and with earlier general circulation experiments. The main weaknesses of the calculation are the level-of-no-motion assumption (which is particularly questionable in high latitudes) and the neglect of form drag on the Bering Strait sill.

Table of Contents:

- [Introduction](#)
- [Where is the northward](#)
- [Quasi-island theory](#)
- [The diamond model and](#)
- [Numerical simulations](#)
- [Discussion and conclusions](#)
- [REFERENCES](#)
- [APPENDIX](#)
- [FIGURES](#)

Options:

- [Create Reference](#)
- [Email this Article](#)
- [Add to MyArchive](#)
- [Search AMS Glossary](#)

Search CrossRef for:

- [Articles Citing This Article](#)

Search Google Scholar for:

- [Doron Nof](#)

1. Introduction

It is common among oceanographers to argue that the formation of North Atlantic Deep Water (NADW) is intimately


connected to a compensating upwelling in the Pacific and Indian oceans (Stommel and Arons 1960, 1972; Munk 1966; Broecker 1991). In this scenario, the rapidly falling water and the slowly rising water are zonally connected via the Southern Ocean and the so-called great global conveyor.

According to the traditional way of looking at the conveyor, it is driven primarily by thermohaline processes (with the wind playing a secondary role). Although this has been the view for quite some time, it has never really been demonstrated that the two processes (wind and thermohaline) are, in fact, independent. Using numerical simulations, Toggweiler and Samuels (1995) have pointed out that the southern winds are probably important to the conveyor circulation (implying that the two processes are not entirely independent). Furthermore, it has been recently demonstrated analytically (Nof 2000) that not only are the two processes not entirely independent, but that it is the wind field, rather than the thermohaline processes, that is the main agent controlling the *exchange* between the Southern Ocean and the Atlantic Ocean. This is not to say that thermohaline processes do not control the rate of NADW formation (which they, of course, do) but rather to say that thermohaline processes by themselves can only cause downwelling and upwelling in regions confined by the boundaries of the Atlantic basin; that is, they can only cause vertical exchange within the limits of the Atlantic Ocean.

This is so because the transport from the Southern Ocean into the South Atlantic, across a section connecting the tip of South America with the tip of South Africa, is determined by the sea level and the wind stress along this cross section. It has been shown in Nof (2000) that the sea level difference between the two outer edges of the above section is determined by the wind stress along the contour (containing the Americas and the Atlantic Ocean) and not the cooling rate over the North Atlantic. In what follows I shall use a similar approach to examine the exchange between the Pacific–Indian Ocean system and the Southern Ocean.

a. Approach

Following that of Nof (2000), the approach presented here involves integration of the linearized momentum equations over the pseudo island and the surrounding ocean. “Pseudo island” is defined here as a continent (containing Africa, Europe, and Asia) that is surrounded by open water but does not have any net flow around it. For most of the integration contour, a level of no motion that lies somewhere between 500 and 1500 m is assumed, and the density is allowed to vary in space (i.e., the density of the entire moving layer is allowed to change). The speeds below the level of no motion are negligible (in comparison with the speeds in the upper layer), but, because the thickness of the nearly stagnant water is very large (say 4000 m), the transport is not necessarily small (e.g., Gill and Schumann 1979). Because there is almost no (observed) flow through the Bering Strait, the transport through it is taken to be zero, implying that all waters that enter the Indian–Pacific system are required to increase their density, sink to a level below the level of no motion, and return southward to exit the basins. (This also implies that it is not necessary to make the level-of-no-motion assumption in the shallow Bering Strait and its immediate vicinity, because in this region the entire column is taken to be at rest.)

The above scenario corresponds to a “shallow” meridional overturning cell (MOC). The term shallow is used here in the sense that it does not involve surface water sinking all the way to the bottom but rather upper water that returns southward at middepth somewhere between the level of no motion and the bottom (Fig. 1 ). The model involves two layers: an active continuously stratified upper layer [containing both thermocline (whose density corresponds to $\sigma_\theta < 26.20$ in midlatitude) and intermediate water (whose density corresponds to $26.20 < \sigma_\theta < 27.50$ in midlatitude)] and an inert deep layer (whose density corresponds to $27.50 < \sigma_\theta < 27.90$ in midlatitude). Because of heat exchange and diapycnal mixing, this lower boundary does not necessarily coincide with a particular isopycnal. The lower boundary of the active layer is defined here as the top of the layer whose velocities (but not necessarily the transports) are negligibly small.

Heat exchange between the intermediate water and deep water is allowed, but the details of this exchange do not have to be specified. Africa is considered to be a part of the island continent (even though it is actually surrounded by water) because the precise sea level drop along the Suez Canal connecting the Mediterranean and the Red Sea is not known.

Although the mass flux through the canal is obviously negligible [$O(100\text{--}1000 \text{ m}^3 \text{ s}^{-1})$], the frictional head loss associated with the canal is not necessarily small because of its relatively small cross section (approximately $300 \text{ m} \times 15 \text{ m}$) and its longitudinal extent $O(100 \text{ km})$. Using the Manning's formula (discussed later in section 6b(1), one finds that the head loss can reach as much as 30 cm. The Gibraltar Strait is also taken to be closed on the ground that the mass flux through it (about 1 Sv; $\text{Sv} \equiv 10^6 \text{ m}^3 \text{ s}^{-1}$) is small when compared with the fluxes of interest here [$\sim O(10 \text{ Sv})$].

The model is *diagnostic* in nature (rather than *prognostic*) because there is no known dynamical reason for the flow through the Bering Strait to be zero. With a depth of 50 m and a width of 150 km, the strait could easily have transferred 10 Sv or much more (if the hydraulic capacity were considered). The fact that it does not transfer a significant amount of mass is merely a reflection of the manner by which the wind, diapycnal mixing, and thermohaline processes are combined.

Using quasi-linear dynamics, a simple transport formula is derived. It shows that the northward transport of upper and intermediate water into the Pacific and Indian Oceans is determined solely by the wind field and the geography of the basin.

It is given by $\oint \tau \cdot f_0 \rho_0 d$, where τ is the wind-stress component along the integration path (which includes the pseudo island and the ocean to the east), f_0 is the (average) Coriolis parameter along the southernmost section of the path, and ρ_0 is a reference density. Detailed application of this transport formula (which includes the western boundary current, the Ekman transport, and the interior geostrophic transport underneath) to the combined Pacific–Indian Ocean system using actual geography and spherical coordinates as well as actual meridional and zonal winds [adopted from 40-yr averages given by the National Centers for Environmental Prediction (NCEP 1999)] gives 18 Sv for the transport of upper water into the two oceans.

For clarity, three models, with an increasing degree of geographic complexity, will be presented. The first model consists of a rectangular meridional continent subject to zonal winds only (Fig. 2) and is essentially identical to that in Nof (2000) except that the MOC is not extended all the way from the surface to the bottom. The second model contains a continent whose shape resembles a diamond (Fig. 3). I find that such a model is helpful because the Africa–Asia continent is very broad and it is difficult to argue that it is a “thin quasi-island.” [This diamond model was not considered in Nof (2000).] The diamond model also includes a gap with a sill corresponding to the shallow topography of the Bering Strait. [This aspect was also absent from Nof (2000).] The third model (Fig. 4) includes 1) meridional winds, 2) the sphericity of the earth, and 3) the actual geometry of the boundaries. This is followed by presenting process-oriented numerical experiments and comparing them with the transport formula for the diamond model (the second model). It is mentioned here in passing that the two simplified models that are introduced might appear at first to be irrelevant because they are very simple when compared with the third “realistic” model that shall ultimately be used. Although this is definitely true, their introduction is necessary because it helps to identify the processes in question.

The main difference between the numerical model presented in Nof (2000) and the present numerical work is in the geometry and the sill that extends all the way from the bottom to approximately 7% of the upper-layer undisturbed thickness (corresponding to the bottom topography in the Bering Strait). [Note that, because an attempt has been made to make the present article self-contained, there is some minimal (unavoidable) overlap between the two articles. The overlap is, nevertheless, confined to a brief derivation of the general transport formula presented in section 3.]

b. Limitations

The two main limitations of the general contour integration approach (Fig. 4) are the assumption of a level of no motion (which is particularly questionable in high latitudes) and the neglect of the pressure force acting on the Bering Strait sill (Fig. 5). These two issues shall be taken one by one.

Because the stratification decreases as one goes from the equator to the poles, the level-of-no-motion assumption is becoming less and less justified as one proceeds to high latitudes. The southernmost boundary of our integration contour (section AB in Fig. 4) is deep and well within the permissible range. On this basis, both Veronis (1973) and Godfrey (1989) have used the level-of-no-motion assumption there, and I shall do the same. [Note, however, that farther south, within the Antarctic Circumpolar Current (ACC), the assumption is clearly violated. It is curious that, for the ACC, Munk and Palmén (1951) suggested that most of the sea level drop occurs across the three ridges. However, using satellite data, Gille (1997) argues that, in contrast to Munk and Palmén's analysis (suggesting that much of the form drag encountered by the ACC is due to three ridges), the ACC form drag is more evenly distributed with only 15%–20% of the drag taken up by each of the three ridges.]


Justifying the level-of-no-motion assumption for the northern part of the integration contour (in the vicinity of the Bering Strait) is a different matter, however, because it is relatively shallow (<100 m). Although this could have been a serious problem, it so happened that the flow through the Bering Strait is very small so that one can take the whole column to be a “level-of-no-motion.” Hence, the assumption is also adequate for the northern boundary. (Note that local winds do not act on a large enough area to establish a significant flow through the strait, so their action can have only a small effect on our integration.) This completes the discussion of the level-of-no-motion assumption.

I shall now briefly discuss the second main limitation, that is, the neglect of the pressure force acting on the Bering Strait sill. To see that this could potentially be a problem, it is noted that, even if there is no flow through the strait (so that there is obviously no sea level drop across the strait), there could still be a pressure force exerted on the sill (Fig. 5). To show that this is not a serious issue, I first performed a set of numerical experiments (section 5) with a sill whose dimensions are similar to those of the Bering Strait (i.e., it extends well into the upper layer). These experiments clearly show that, for this calculation, it makes no difference whether there is a sill. Using observations, (section 6) it is then shown that the neglect of this pressure force (i.e., taking the vertically integrated pressure to be continuous) may introduce an error of a few Sverdrups and that this can only subtract from (but not add to) the estimated transport. It is also shown in section 6 that, even though the sea level difference between the North Atlantic and the North Pacific (far away from the Bering Strait) is about 40 cm (Reid 1961), the sea level drop across the Bering Strait itself is entirely insignificant.

In [section 2](#) the issue of what can possibly cause a downward motion in the absence of deep water formation is addressed. In [section 3](#), the thin quasi-island calculation using the most general governing equations is presented. This is followed by a presentation of the intermediate (diamond) model with and without a sill ([section 4](#)) and its comparison to the (three sets of) 34 new numerical simulations ([section 5](#)). The application of the general transport formula to the Pacific–Indian system is given in [section 6](#), which also includes a detailed discussion of the model's weaknesses.


2. Where is the northward transport of upper water going?

A question that comes immediately to mind regarding the surface waters that we say enter the Pacific–Indian system is, how are they removed from these basins? The answer to this question is not trivial because, in contrast to the Atlantic, there is no deep water formation in these basins. Three processes can be responsible for the exchange between upper and lower levels. First, in analogy to conventional wisdom, which states that deep waters leave the Pacific and Indian Oceans because of a distributed upward motion into the thermocline (e.g., [Munk 1966](#)), the water that *enters* the basins can be removed by distributed *downward* vertical motion at (or below) the level of no motion.

To see that this is plausible, recall that the vertical component of the steady heat diffusion equation is $wT_z = kT_{zz}$, where w is the vertical velocity, T is the temperature, and k is the vertical eddy diffusivity. When the curvature of the temperature profile is positive ($T_{zz} > 0$), the fluid is heated from above and the vertical velocity is positive. This situation corresponds to an upwelling associated with a balance between a downward diffusion of heat and an upward advection. It corresponds to the conventional wisdom associated with an upwelling into the upper waters. By contrast, when T_{zz} is less than 0, the ocean is cooled from below [by the Antarctic Bottom Water (AABW)] and the diffusion equation implies that w is negative. That such downward velocity is plausible at this depth was already recognized by [Warren \(1977\)](#), who determined that the curvature of the density profile (at 1–4 km) in the Pacific changes sign with depth somewhere between the thermocline and the bottom (see [Fig. 6](#) ).

As already pointed out by [Warren \(1977\)](#), the downward motion in the Pacific does not negate the conventional upward motion into the thermocline because the latter occurs higher in the water column. Taking the horizontal scales of the combined Pacific–Indian basin to be 25 000 km by 10 000 km with an (admittedly small) vertical variation scale of, say, 500 m, one finds that an average vertical diffusivity of approximately $0.3 \text{ cm}^2 \text{ s}^{-1}$ is sufficient to force the 18 Sv downward (to a depth below the level of no motion). This vertical eddy diffusivity is too high when compared with recent measurements (e.g., [Ledwell et al. 1993](#)) but is an order of magnitude smaller than average estimates given by [Ganachaud and Wunsch \(2000\)](#), suggesting that the sinking may be localized.


The second possible way for the conversion (of upper to intermediate water) to take place is via eddy fluxes (e.g., [Gnanadesikan 1999](#)). There is still one more possibility for the conversion and it is the familiar air–sea exchange in the North Pacific. This can lead to the formation of intermediate water that constitutes a part of our MOC. At this point it is difficult to decide which of the three possible processes is the most important one. In this context the reader is also referred to [Samelson \(1999\)](#).

It is important to realize that the idea of a shallow MOC in the Pacific and the above downward motion arguments are consistent with the earlier inverse calculations of [Wunsch et al. \[\(1983\), see their Fig. 10\]](#), with the conventional wisdom regarding silicate distribution, and with earlier general numerical simulations ([Hallberg and Toggweiler 1998](#)). To see that this is what the silicate distribution ([Fig. 7](#) ) implies, note that an upward motion from the bottom to a midlevel of about 3000 m (and not all the way to the surface) implies a downward motion from above (to compensate for the warming of the water carrying the silicate). Using a 12-layer model, [Hallberg and Toggweiler \(1998\)](#) reproduced the above-mentioned deep cell (represented by the silicate distribution); an adjacent upper cell (of the kind about which I speak) carrying 5–15 Sv was also observed in their experiments. With small ($0.1 \text{ cm}^2 \text{ s}^{-1}$) thermocline diffusivities and large deep diffusivities (due to tides or topography-induced mixing), the heat exchange between the cells is primarily due to mixing and the upper and lower cells are of the same magnitude (i.e., both carry 5–15 Sv). For completeness, the reader is also referred to [Klinger and Marotzke \(1999\)](#), who showed that a shallow buoyancy-induced cell is dynamically possible.

3. Quasi-island theory

For clarity, the derivation of the formula used in [Nof \(2000\)](#) and in the present calculations is now very briefly reviewed. The governing equations that I shall use are essentially the same as in [Godfrey \(1989\)](#) except that I show more explicitly that, within the moving upper layer, the density ρ can be a function of x , y , and z , implying that thermohaline processes are included. Underneath the upper moving layer there is not only a *surface* of no motion but there is also a very thick intermediate layer (below the moving layer) whose speeds (but not necessarily the transports) are small when compared with those of the upper moving layer. Furthermore, transports of $O(1)$ might be exchanged (within the integration area)

between the thick layer (density ρ_0) and the upper moving layer ($\rho \leq \rho_0$). It is important to realize at this point that all of the equations need to hold *only along the boundary of integration*. Within the integration region, other equations may hold. Also, note that the main difference between this analysis and that of [Godfrey \(1989\)](#) is the inclusion of diabatic processes, which, as we shall see, prevent any flow through the northern gap (the Bering Strait).

Consider now the first (simplified) model containing the straight pseudo island ([Fig. 2](#) ). The upper moving layer is continuously stratified and is subject to both zonal wind action and diabatic processes. A vertically integrated pressure, $P^* = \int_{-\xi}^{\eta} P dz$, is defined, where ξ is the depth below which the horizontal pressure gradients are small and negligible, η is the free surface vertical displacement (measured positively upward), and P is the deviation of the hydrostatic pressure from the pressure associated with a state of rest. Namely,

$$\partial P / \partial z = \rho' (x, y, z)g,$$

where the density ρ is given by

$$\rho = \rho_0 + \bar{\rho}(z) + \rho' (x, y, z),$$

with ρ_0 being the (uniform) density of the lower layer, $\bar{\rho}(z)$ the density deviation associated with a motionless upper layer, and $\rho' (x, y, z)$ the density deviations associated with the motions of the stratified upper layer. For convenience, all variables are defined both in the text and in the [appendix](#).

Using Leibniz's formula for the differentiation under the integral, one can show that, because $P = 0$ at $z = \eta - \xi$, vertical integration of the linearized Boussinesq equations from $-\xi$ to η gives

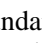
$$-fV = -\frac{1}{\rho_0} \frac{\partial P^*}{\partial x} + \frac{\tau^x}{\rho_0} \quad (3.1)$$

$$fU = -\frac{1}{\rho_0} \frac{\partial P^*}{\partial y} - RV, \quad (3.2)$$

where U and V are the vertically integrated transports in the x and y directions (pointing eastward and northward, respectively) and R is an interfacial friction coefficient, which need not be specified for the purpose of this analysis. Here, f is the Coriolis parameter (varying linearly with y), and τ^x is the wind stress in the x direction. Both ξ and η are functions of x and y so that the level of no motion can be, say, 500 m in one part of the ocean and 800 m in another. Note that U and V include both the Ekman transport and the geostrophic transport underneath.

Recall that the no-motion-in-the-lower-layer assumption merely requires the velocities and not necessarily the transports to be small. This is so because the vertical integration is done over the upper layer and not the lower layer. [This conclusion was first reached by [Gill and Schumann \(1979\)](#)]. We shall see shortly that this is consistent with the lower limb of the suppressed MOC returning southward along the western boundaries outside the Sverdrup balance regime.

In this model, energy is supplied by both the wind and heat exchange; dissipation occurs through interfacial friction within the limits of the western boundary current system (such as the Kuroshio and the Agulhas). Interfacial friction is not present in [\(3.1\)](#) because RU is small and negligible. Furthermore, because the velocities are small in the ocean interior, the frictional term is negligible there. The boundary condition along the solid boundaries is, of course, the familiar no-normal flow into the western and eastern walls. Because $U \equiv 0$ along the two eastern boundaries (BD and A' C') it follows immediately from [\(3.2\)](#) with $RV \equiv 0$ that the vertically integrated pressure P^* is constant along both BD and A' C' .

We now integrate [\(3.1\)](#) from the western tips of the pseudo island to the eastern boundary (i.e., [sections 1 and 2](#) shown in [Fig. 2](#) ), noting that there is no transport through cross section AB because, in line with the no-flow-through-the-Bering-Strait assumption, all the surface water that enters through CD is required to sink prior to reaching AB. The result is


$$0 = -\frac{1}{\rho_0}(P_B^* - P_A^*) + \int_A^B \left(\frac{\tau^x}{\rho_0} \right) dx, \quad \text{and} \quad (3.3)$$

$$-f_2 Q = -\frac{1}{\rho_0}(P_D^* - P_C^*) + \int_C^D \left(\frac{\tau^x}{\rho_0} \right) dx, \quad (3.4)$$

where Q is the net meridional transport across CD, f_2 is the Coriolis parameter along [section 2](#), and the subscripts A , B , C , and D denote the location of the variable in question.

By subtracting [\(3.4\) from \(3.3\)](#) and taking into account the eastern boundary condition, and by taking the island to be narrow (i.e., $P_C^* = P_{C'}^*$, $P_A^* = P_{A'}^*$), one finds the simple relationship,

$$Q = -\frac{1}{f_2} \left(\int_C^D \frac{\tau^x}{\rho_0} dx + \int_B^A \frac{\tau^x}{\rho_0} \right), \quad (3.5)$$


which is the desired formula for the simplest first model ([Fig. 2](#) ). It gives the combined (wind and thermohaline) transport in terms of the wind field and the geography alone.

Although [\(3.5\)](#) resembles the familiar expression for the Ekman transport, it actually includes the Ekman transport, the geostrophic flow underneath, and the western boundary current (WBC) transport. It so happens that the interior geostrophic transport cancels the WBC transport so the net amount is *equal* to the Ekman transport. It is important to realize that this does not at all mean that the transport is caused by an Ekman flow, because the water masses in the three components (WBC, geostrophic interior, and Ekman flow) are not necessarily identical.

Five additional comments should be made with regard to [\(3.5\)](#). First, in the limit of no diabatic processes (i.e., no heat exchange and no diffusion), the wind would attempt to force all the water through the Bering Strait, hydraulic control, and jumps (e.g., [Whitehead 1998](#)) or large frictionally induced pressure gradients across the gap would be present and, as a result, the model would break down. Second, in the limit of very strong cooling (from below), there will be more total downwelling than that given by [\(3.5\)](#) but there will also be more compensating upwelling (somewhere else in the Pacific–Indian system) with the final outcome of no change in the *net* import or export. Third, in the limit of no wind ($\tau^x \equiv 0$), no water can get in and out of the basin and whatever downwells has to upwell elsewhere within the basins themselves. Fourth, in the limit of very strong winds, some of the water will again be forced via the Bering Strait into the Atlantic. As in the first point above, the model breaks down in this case. Fifth, it is important to realize that the integral of both the pressure gradient and the gradient of the vertically integrated pressure vanish when the integration is done along a closed contour (provided, of course, that both are continuous along the contour).

4. The diamond model and the realistic model

It is a simple matter to extend the results of the simple straight island model to both the diamond model (which will be used later for the numerical simulations) and to the more realistic model containing meridional winds and more complicated geometry (the third model that will be used for this application). Using again the Boussinesq approximation and the vertically integrated equations in spherical coordinates, one ultimately arrives at the (earlier mentioned) most general transport formula,

$Q = \oint \tau^x dl / (-f_0 \rho_0)$, where l is the closed integration path (which contains the pseudo island and the ocean to its east) and f_0 is the average Coriolis parameter along cross section AB ([Fig. 4](#) ).

Recall that only two boundary conditions entered the derivation of this general formula. The first is the no flow into the boundary condition. This essentially implies that, along the eastern boundary, the vertically integrated pressure gradient is balanced by the wind stress, that is, $\partial P^* / \partial x = \tau^x$. This condition was verified by [Godfrey \(1989\)](#) for most of the world's eastern boundaries using the Levitus data. Because P is the deviation of the hydrostatic pressure from the pressure associated with a state of rest (i.e., $\partial P / \partial z = -\rho' g$), and because $P^* = \int_{\xi}^{\eta} P dz$, it is clear that the cooling and warming (which the fluid experiences as it flows away or toward the equator) enter the problem through ρ' and P so that it is included in the calculation (and in Godfrey's verification). Note here that Godfrey's verification implies that the role of *frictional* eastern boundary currents is secondary, that is, it can be neglected to first order. Furthermore, it is important to realize that the present eastern boundary condition is consistent with the cooling spirals (and the induced upwelling and downwelling) of [Spall and Pickart \(2001\)](#) because the two models have the same (inviscid) dynamics. For instance, in the

absence of an alongshore wind, there is a long-wall pressure gradient in Spall's upper layer but it is compensated for by an opposite gradient in the lower layer so that the total gradient is zero as is the case in our vertically integrated model.

The second boundary condition that was used in the derivation of (3.5) is no (vertically integrated) pressure gradient across the gap. Surely, this second condition would be violated if there were a frictionally dominated flow through the gap. As mentioned, however, the focus here is on the limit at which there is no such flow through the gap and, if there is no flow through the gap, then there is, of course, no pressure drop across it. We shall see later in section 6 that both the numerical simulation and estimates of the actual sea level drop clearly support this assumption.

5. Numerical simulations

Instead of verifying the above general transport formula using very complicated numerical models (corresponding to Fig. 4), the formula's application to the diamond model (which does not contain meridional winds) was examined. To do so, an application of a Bleck and Boudra “reduced-gravity” isopycnic model (Bleck and Boudra 1981, 1986; Bleck and Smith 1990) was used. Namely, the upper-layer density was taken to be constant in the numerical simulations. To represent the meridional transport, a (mass flux) source in the southeast corner and a sink in the northern basin were introduced. The mass flux associated with this source and sink is not specified ahead of time. Rather, the wind was allowed to blow, the transport initially established across CD (Fig. 3a) was measured, and then the source and sink were required to accommodate this measured transport. This process was repeated and the sink and source fluxes were continuously adjusted until a steady state was reached.

Three sets of experiments (sets A, B, and C) totaling 34 experiments were performed. First, to verify that the computed transport is independent of the gap width, a set of experiments in which only the gap width was varied was initially performed (set A). Second, to verify that the presence of a sill across the gap is not important, the varying-gap experiments (set A) were repeated with a sill extending all the way from the bottom to 40 m from the free surface [approximately 7% of the total undisturbed depth of 600 m (set B)]. This sill depth corresponds to the situation associated with the Bering Strait. We shall see that the results of the sill and no-sill experiments were virtually indistinguishable, indicating that the sill is not important to our calculation. Third, the wind stress was varied, the transport was again measured and adjusted, and the theoretically computed transport versus the numerical transport was then plotted (set C).

The sill was implemented by keeping the upper-layer depth fixed (at 40 m) within the gap itself and leaving the depth north and south of the gap free. Hence, the presence of the sill enters the momentum equations directly only through the lateral friction terms. (Indirectly, it enters through the speeds and pressure.) In a similar way, it directly enters the continuity equation by restricting the volume flux through the gap. (Note that the velocity and pressure adjust each other across the gap.) Of course, a more thorough investigation of the sill problem should include the continental slopes, but that is beyond the scope of this study.

To make the runs more economical, a magnified β (and a magnified wind stress τ) and a reduced basin size were used. Fig. 8 shows the observed (numerical) transports and their relationship to the analytics for the varying-gap case with and without a sill (sets B and A). It displays a good agreement of the nonlinear numerical simulations and the quasi-linear analytical computation no matter how narrow the gap is. Figure 9, which shows the experiments of varying wind stress, also displays a good (but not excellent) agreement of the analytics with the numerics (set C). The numerical data presented in Fig. 9 displays a clear systematic bias in the gradient of the lines; I unfortunately was unable to determine its cause.

6. Discussion and conclusions

For the actual transport into the Pacific–Indian system calculations, NCEP (1999) reanalysis data were used for annual mean winds (averaged over 40 yr) with a drag coefficient of 1.6×10^{-3} [which is the appropriate coefficient for such winds with a speed of less than 6.7 m s^{-1} (e.g., Hellerman and Rosenstein 1983)]. Along the chosen realistic path (Fig. 4), the integration was done over $2^\circ \times 2^\circ$ boxes. With the aid of the general transport formula, one finds a net meridional transport of about 18 Sv. All the high-latitude (northern) coastlines were taken to be ice free, but including ice and assuming no wind stress transfer across it makes practically no difference because 90% of the (calculated) 18 Sv transport is due to the strong southern winds.


a. General remarks

The answer to the question posed in the title of this article is: yes, there should be a (shallow) MOC in the Pacific and Indian Oceans. The cell is primarily controlled by the wind, but thermohaline processes determine its detailed structure. It is argued that the 18 Sv (± 5 Sv) that are carried northward along the surface *downwell* within the confines of the Pacific and Indian Oceans somewhere between 500 and 3000 m. This does not necessarily contradict the idea that there must be an upwelling of some *deep* water into the upper layer nor does it negate the idea that intermediate water upwells into the thermocline, because such flows can be simply superimposed on our proposed circulation pattern.

The analysis shows that the *net* amount entering the South Pacific and the Indian Ocean from the Southern Ocean is controlled by the wind. According to the calculation, thermohaline processes and buoyancy fluxes do control the thermohaline circulation but have no bearing on the exchange via the cross sections connecting the tip of South Africa to the tip of South America; that is, they can only cause sinking and upwellings that are confined to the limits of the Pacific and Indian Oceans. In other words, thermohaline processes by themselves cannot draw water into these oceans because the amount of this drawn water depends on the sea level difference between the two edges of the above-mentioned southern cross section (controlled by the wind along the integration contour) and the local wind stress.

b. Weaknesses

As in most models, there are a few potentially serious weaknesses in our model. Many of these weaknesses are in one way or another related to the shallow Bering Strait. (The issue of whether the level-of-no-motion assumption is adequate here was already discussed in the introduction and does not need to be repeated here.) Because both our analytical and numerical models with or without a sill consider the limit of no flow through the modeled Bering Strait, there was no sea level drop across it (in both models), implying that the theory is valid and self-consistent. The applicability of the models to the ocean is another matter, however, and, as we shall shortly see, it is not so simple to tell how valid the applicability is to the real world.

In what follows I shall address two different observational aspects of the no-flow-through-the-Bering-Strait assumption. First, I shall examine whether the sea level drop across the strait (neglected in our calculations) could be important. Second, I shall examine how important the actual pressure exerted on the Bering Strait sill is (again neglected in our calculation). [Note that it has already been demonstrated numerically (Fig. 8 ) that the latter is not important.] This second aspect of a pressure on the sill needs to be distinguished from the first one (sea level drop) because the two aspects are independent of each other.

1) IS THE ACTUAL SEA LEVEL DROP ACROSS THE BERING STRAIT NEGLIGIBLE?

To examine this question, note that an upper bound of the sea level drop can be obtained using the so-called Manning's formula that is traditionally used by engineers (e.g., [Chow 1959](#); [Giles 1962](#); [Chaudry 1993](#)) to estimate the frictionally induced downstream pressure gradient along rivers but is also used by geologists to estimate the flow from the paleo-Mediterranean Sea to the (then freshwater lake) Black Sea and to estimate the draining from glacier Lake Agassiz. For this purpose, the Bering Strait is taken to be 150 km broad, 50 m deep, and 150 km long and the Manning's frictional coefficient n is taken to be as large as one can reasonably expect (0.03). Assuming that about 1 Sv goes through the strait to estimate the speed, one finds with the aid of Manning's formula an along-strait sea level drop of less than 1 cm, an amount that is certainly negligible when compared with the 30–60 cm required to drive our MOC. (Note that, as in any other boundary current, it is assumed here that the flow in the Bering Strait is in a cross-stream geostrophic balance and along-stream frictional balance.) A still-smaller estimate of 10^{-2} mm is obtained by following the traditional oceanographic approach of vertically integrating the relationship

$$g \frac{\partial \eta}{\partial y} = \frac{1}{\rho_0} \frac{\partial \tau}{\partial z}$$

and taking the bottom stress divided by ρ to be $C_D(u^*)^2$, where C_D , the (dimensionless) drag coefficient, is 1.6×10^{-3} and u^* , the frictional velocity, is about 3% of the average speed above. We see that both methods show that the no-pressure-gradient-in-the-Bering-Strait assumption is adequate.

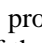
2) IS THE VERTICALLY INTEGRATED PRESSURE CONTINUOUS ACROSS THE BERING STRAIT?

Because a continuous sea level does not necessarily assure a continuous vertically integrated pressure (see [Fig. 5 !\[\]\(f95dab70c751fda7d824b8b03650f7aa_img.jpg\)](#)), I shall now address the question of whether the deep pressure gradient that can be supported by the (relatively shallow) Bering Strait bottom topography (neglected in our calculation) can be important. It is easy to see that in the quasigeostrophic limit (i.e., *small* interface displacement as compared with some mean mutual depth of the moving layers in the two adjacent oceans), the vertically integrated pressure should be taken to be continuous across the (almost stagnant) strait even though the interfaces strike the bottom at different depths on the two sides of the strait. However, the interface displacements in the vicinity of the Bering Strait are not consistent with the quasigeostrophic approximation because the associated amplitude is not small. For example, the 1.027 density contour shoals from 300 m south of the strait to 100 m north of the strait ([Gorshkov 1983](#), 129–130), implying large vertical excursions. By taking a $\Delta\rho/\rho$ of 0.75×10^{-3} for the density difference between the upper water (at, say, 100 m) and deeper water (at, say, 500 m), a Coriolis parameter of 10^{-4} s^{-1} , a mean depth of 300 m, and an amplitude of 200 m, one gets (through the geostrophic transport relationship) that the error introduced by considering the vertically integrated pressure to be continuous is about 2 Sv.

It is easy to show that, because the density surfaces shoal as one proceeds from the Pacific to the Arctic, the pressure on the sill opposes the counterclockwise wind stress along the constant so that the error introduced by the neglect of the topographic pressure can only *subtract* from our estimate of the transport (a few or several Sverdrups at the most) but cannot add to it. [Note here in passing that it would add to our calculation for the Atlantic presented in [Nof \(2000\)](#) because the Atlantic integration is done in an opposite sense to that of the Pacific–Indian integration.]

c. Final remarks

An additional potential weakness of the model's applicability is the lack of direct observational support. Although this is definitely a weakness, the Pacific–Indian system is so large and there are so many places that it can go in and out of the basins and so many places that upwelling and downwelling can occur that one may not see the 18 ± 5 Sv transport unless one is specifically looking for it. Given the indirect observation support (in terms of inverse calculations and silicate distribution) discussed earlier in the end of [section 2](#), this weakness is not viewed as critical.

Four final comments should be made about the analysis. First, although the flow does not specifically have a barotropic component (by barotropic, it is meant here a velocity component extending all the way from the top to the bottom) one can, at least qualitatively, think of simply superimposing such a flow. Because there is (almost) no flow through the Bering Strait, any barotropic flow entering the South Atlantic from the Southern Ocean must also exit the South Atlantic. It consequently can have only a minimal effect on the MOC. Second, there is no contradiction between the conclusions and the traditional calculations showing a leakage of warm Agulhas water into the South Atlantic (e.g., [Macdonald 1998](#); [Ganachaud and Wunsch 2000](#)) because such a flow pattern can simply be superimposed on the MOC. Third, traditional island-rule calculations used to compute the Indonesian throughflow or other bodies of water (e.g., [Godfrey 1989](#); [Wajsowicz 1993](#); [Pedlosky et al. 1997](#); [Pratt and Pedlosky 1998](#); [Firing et al. 1999](#); [Liu et al. 1999](#)) ignore water conversions (and upwelling and downwelling), which are the main focus of the study. Note that such calculations usually take the integration lines east of the island to be zonal; this cannot be done in this problem [because of the geography, ([Fig. 4](#) )], implying that an error of 10%–20% is introduced (through the variation of the Coriolis parameter along the southern portion of the contour).

It should be stressed that, although the Bering Strait is critical for the calculations, it is not at all clear what role the Bering Strait plays in the general oceanic circulation. Both [Toggweiler and Samuels \(1995\)](#) and [McDermott \(1996\)](#) obtain similar numerical results without having a Bering Strait in their simulations. This result may simply be fortuitous, but the fact that the flow through the strait is almost zero (even though it could easily transfer 5–10 Sv) is another indication that much of the Bering Strait general circulation dynamics is not clear.

Acknowledgments

Discussions with S. Gille, P. Robbins, D. Roemmich, K. Speer, and G. Weatherly regarding the observational aspects of the problem were very helpful. Conversations with Robbie Toggweiler and Robert Hallberg regarding the silicate distribution discussed in [section 2](#) and the GCM runs [briefly addressed in [Hallberg and Toggweiler \(1998\)](#)] were also illuminating. This study was supported by the National Science Foundation under Contract OCE 9911324 and 9633655; National Aeronautics and Space Administration Grants NAG5-7630, NGT5-30164, and NAG5-10860; Binational Science Foundation Grant 96-105; and Office of Naval Research Grant N00014-01-0291.

REFERENCES

- Bleck R., and D. Boudra, 1981: Initial testing of a numerical ocean circulation model using a hybrid, quasi-isopycnic vertical coordinate. *J. Phys. Oceanogr.*, **11**, 755–770. [Find this article online](#)
- Bleck R., 1986: Wind-driven spin-up in eddy-resolving ocean models formulated in isopycnic and isobaric coordinates. *J. Geophys. Res.*, **91**, 7611–7621. [Find this article online](#)
- Bleck R., and L. Smith, 1990: A wind-driven isopycnic coordinate model of the north and equatorial Atlantic Ocean. 1. Model development and supporting experiments. *J. Geophys. Res.*, **95**, 3273–3285. [Find this article online](#)
- Broecker W., 1991: The great ocean conveyor. *Oceanography*, **4**, 79–89. [Find this article online](#)
- Chaudry M. H., 1993: *Open Channel Flow*. Prentice Hall, 483 pp.
- Chow V. T., 1959: *Open-channel hydraulics*. McGraw-Hill, 680 pp.
- Craig H., W. Broecker, and D. Spencer, 1981: *Sections and Profiles*. Vol. 4, *GEOSECS Pacific Expedition*, U.S. Government Printing Office, 251 pp.

- Firing E., B. Qiu, and W. Miao, 1999: Time-dependent island rule and its application to the time-varying North Hawaiian Ridge Current. *J. Phys. Oceanogr.*, **29**, 2671–2688. [Find this article online](#)
- Ganachaud A., and C. Wunsch, 2000: Improved estimates of global ocean circulation, heat transport and mixing from hydrographic data. *Nature*, **408**, 456–457. [Find this article online](#)
- Giles R., 1962: *Theory and Problems of Fluid Mechanics and Hydraulics*. McGraw-Hill, 272 pp.
- Gill A. E., and E. H. Schumann, 1979: Topographically induced changes in the structure of an inertial coastal jet: Application to the Agulhas Current. *J. Phys. Oceanogr.*, **9**, 975–991. [Find this article online](#)
- Gille S. T., 1997: The Southern Ocean momentum balance: Evidence for topographic effects from numerical model output and altimeter data. *J. Phys. Oceanogr.*, **27**, 2219–2232. [Find this article online](#)
- Gnanadesikan A., 1999: A simple predictive model for the structure of the oceanic pycnocline. *Science*, **283**, 2077–2079. [Find this article online](#)
- Godfrey J., 1989: A Sverdrup model of the depth-integrated flow for the World Ocean allowing for island circulations. *Geophys. Astrophys. Fluid Dyn.*, **45**, 89–112. [Find this article online](#)
- Gorshkov S., 1983: *Arctic Ocean*. Vol. 3, *World Ocean Atlas*, Pergamon Press, 302 pp.
- Hallberg R., and J. R. Toggweiler, 1998: The ocean's density structure and thermohaline circulation in the limit of weak diapycnal diffusion. *Eos, Trans. Amer. Geophys. Union*, **79**, (Suppl.).
- Hellerman S., and M. Rosenstein, 1983: Normal monthly wind stress over the World Ocean with error estimates. *J. Phys. Oceanogr.*, **13**, 1093–1104. [Find this article online](#)
- Klinger B. A., and J. Marotzke, 1999: Behavior of double-hemisphere thermohaline flows in a single basin. *J. Phys. Oceanogr.*, **29**, 382–399. [Find this article online](#)
- Ledwell J. R., A. J. Watson, and C. S. Law, 1993: Evidence for slow mixing across the pycnocline from an open-ocean tracer-release experiment. *Nature*, **364**, 701–703. [Find this article online](#)
- Liu Z., L. Wu, and H. Hurlburt, 1999: Rossby wave–coastal Kelvin wave interaction in the extratropics. Part II: Formation of island circulation. *J. Phys. Oceanogr.*, **29**, 2405–2418. [Find this article online](#)
- Macdonald A., 1998: The global ocean circulation: A hydrographic estimate and regional analysis. *Progress in Oceanography*, Vol. 41, Pergamon Press, 281–382.
- McDermott D., 1996: The regulation of Northern Hemisphere overturning by Southern Hemisphere winds. *J. Phys. Oceanogr.*, **26**, 1234–1255. [Find this article online](#)
- Munk W., 1966: Abyssal recipes. *Deep-Sea Res.*, **13**, 707–730. [Find this article online](#)
- Munk W., and E. Palmén, 1951: Note on the dynamics of the Antarctic Circumpolar Current. *Tellus*, **3**, 53–55. [Find this article online](#)
- NCEP., 1999: NCEP–NCAR 40-Year Reanalysis dataset. NOAA–CIRES Climate Diagnostics Center. [Available online at <http://www.cdc.noaa.gov>].
- Nof D., 2000: Does the wind control the import and export of the South Atlantic? *J. Phys. Oceanogr.*, **30**, 2650–2667. [Find this article online](#)
- Pedlosky J., L. J. Pratt, M. A. Spall, and K. R. Helfrich, 1997: Circulation around islands and ridges. *J. Mar. Res.*, **55**, 1199–1251. [Find this article online](#)
- Pratt L., and J. Pedlosky, 1998: Barotropic circulation around islands with friction. *J. Phys. Oceanogr.*, **28**, 2148–2162. [Find this article online](#)
- Reid J. L., 1961: On the temperature, salinity and density differences between the Atlantic and Pacific Oceans in the upper kilometer. *Deep-Sea Res.*, **7**, 265–275. [Find this article online](#)
- Samelson R., 1999: Geostrophic circulation in a rectangular basin with a circumpolar connection. *J. Phys. Oceanogr.*, **29**, 3175–3184. [Find this article online](#)
- Spall M., and R. Pickart, 2001: Where does dense water sink? A subpolar gyre example. *J. Phys. Oceanogr.*, **31**, 810–826. [Find this article online](#)

Stommel H., and A. Arons, 1960: On the abyssal circulation of the World Oceans—II. An idealised model of the circulation pattern and amplitude in oceanic basins. *Deep-Sea Res.*, **6**, 217–233. [Find this article online](#)

Stommel H., 1972: On the abyssal circulation of the World Ocean—V. The influence of bottom slope on the broadening of inertial boundary currents. *Deep-Sea Res.*, **19**, 707–718. [Find this article online](#)

Toggweiler J. R., and B. Samuels, 1995: Effect of Drake Passage on the global thermohaline circulation. *Deep-Sea Res.*, **42**, 477–500. [Find this article online](#)

Veronis G., 1973: Model of World Ocean circulation: I. Wind-driven, two layer. *J. Mar. Res.*, **31**, 228–288. [Find this article online](#)

Wajsowicz R. C., 1993: The circulation of the depth-integrated flow around an island with application to the Indonesian Throughflow. *J. Phys. Oceanogr.*, **23**, 1470–1484. [Find this article online](#)



Warren B., 1977: Shades of deep density-depth curves. *J. Phys. Oceanogr.*, **7**, 338–344. [Find this article online](#)

Whitehead J. A., 1998: Topographic control of oceanic flows in deep passages and straits. *Rev. Geophys.*, **36**, 423–440. [Find this article online](#)

Wunsch C., D. Hu, and B. Grant, 1983: Mass, heat, salt and nutrient fluxes in the South Pacific Ocean. *J. Phys. Oceanogr.*, **13**, 725–753. [Find this article online](#)

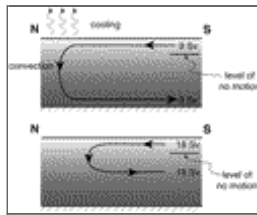
APPENDIX

7. List of Variables

C_D	Dimensionless drag coefficient
f	Coriolis parameter varying linearly with y
f_0	Average Coriolis parameter along cross section AB (Fig. 4 )
f_2	Coriolis parameter along section 2 (Fig. 2 )
g'	“Reduced gravity” $(\Delta\rho/\rho)g$
h	Upper-layer thickness
k	Vertical eddy diffusivity
n	Manning's frictional coefficient
P	Deviation of the hydrostatic pressure from the pressure associated with a state of rest
Q	Net meridional transport across the ocean
R	Interfacial friction coefficient
η	Free surface vertical displacement
$\rho' (x, y, z)$	Density deviation associated with the moving upper layer
$\bar{\rho}(z)$	Density deviation associated with a resting upper layer
ρ_0	Uniform density of the motionless deep water

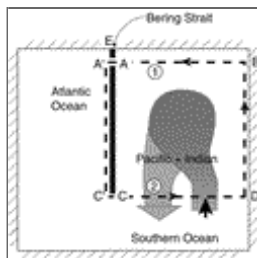
τ	Magnified wind stress
T	Temperature
τ ; ℓ	Actual wind stress along the integration path ℓ
τ^x	Wind stress in the x direction
U and V	Vertically integrated transports in the x and y direction
u^*	Frictional velocity
w	Vertical velocity
x	East–west direction
y	North–south direction
ξ	Depth of the level of no horizontal pressure gradient
z	Vertical direction

Figures



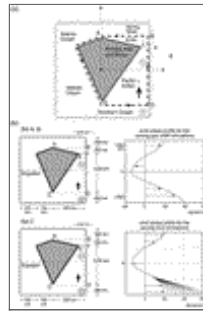
[Click on thumbnail for full-sized image.](#)

FIG. 1. Schematic diagram of (top) the familiar Atlantic MOC and (bottom) the suggested (shallow) Pacific–Indian MOC

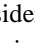




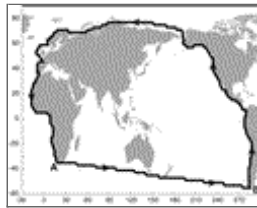
[Click on thumbnail for full-sized image.](#)

FIG. 2. A top view of the straight pseudo-island model. The continent is represented by a narrow meridional pseudo island; the Pacific and Indian Oceans are connected to the Atlantic via a narrow gap (representing the Bering Strait) that allows the pressure to be continuous around the continent but does not allow significant flow through it. (This very simple geometry is used merely for the clarity of the presentation.) The situation corresponds to both thermocline and intermediate waters that are driven meridionally by both zonal winds and thermohaline processes. The thick meridional arrow across CD indicates water entering (exiting) the Pacific and Indian Oceans (from the Southern Ocean). This water downwells (upwells) within the confines of the basin. Points A and A' (as well as C and C') correspond to the eastern and western edges of the continent's northern (southern) tip. The thick broken line (passing on the left-hand side of the pseudo island) denotes the closed integration path. In this simple model the “island” is thin so that $P_A = P_{A'}$ and $P_C = P_{C'}$



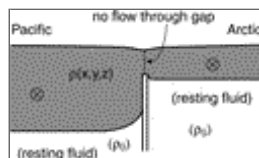
Click on thumbnail for full-sized image.

FIG. 3. (a) A top view of the second pseudo-island model. This “diamond” model is of intermediate complexity in the sense that it is more complicated than the straight meridional wall model considered in [Nof \(2000\)](#) (i.e., [Fig. 2](#) ) and yet is simpler than the actual model that shall be adopted later (i.e., the third model shown in [Fig. 4](#) ). The source \oplus and sink \ominus are situated outside and inside the integration contour. As in the simple model shown in [Fig. 2](#) , the orientation of the surface flow (in or out of the basin) is not determined in advance but rather is found as a part of the problem. Namely, in our numerical simulations the source can act as a sink and vice versa. In this model, the Bering Strait (EF) contains a sill (dotted line) extending all the way from the bottom up to about 7% (40 m) of the upper-layer undisturbed thickness (600 m). [Such a sill is absent from the thin island runs reported in [Nof \(2000\)](#).] (b) Schematics of the (1.5 layer) source-sink numerical experiments and the magnified (and simplified) zonal wind stress as a function of latitude (adapted from [Hellerman and Rosenstein 1983](#)). The model has no thermodynamics. However, because the source \oplus and the sink \ominus are situated in relatively sluggish regions away from western boundary currents, the mass flux exiting the source and entering the sink also represent a reasonable first-order approximation of the thermodynamics. The mass flux was not specified ahead of time. Rather, we let the wind blow for awhile, measured the transport across CD, and then required both the sink and the source to accommodate the measured amount. This procedure was then repeated continuously, and the source mass flux was continuously adjusted until a steady state was reached. (top right) The (fixed) wind profile used for the variable gap width w with and without a sill (sets A and B). (bottom right) The variable wind profile (set C)



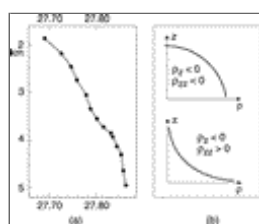
Click on thumbnail for full-sized image.

FIG. 4. A diagram of the closed integration path used in the third, realistic model



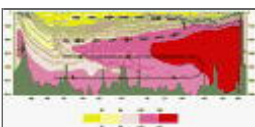
Click on thumbnail for full-sized image.

FIG. 5. A schematic diagram of an idealized Bering Strait with a sill protruding well into the upper layer. The configuration shows that, even when there is no flow through the strait and the lower layer is of the same density in the two oceans, there can still be a force on the sill (due to along-sill geostrophic flow or other processes) so that the vertically integrated pressure is discontinuous, violating our calculation. Numerical simulations with such an idealized sill ([section 5](#)) show that the discontinuity in the vertically integrated pressure is insignificant. Observations ([section 6](#)), on the other hand, suggest that the error introduced by taking the vertically integrated pressure to be continuous (i.e., neglecting the discontinuity and neglecting the fact that the lower-layer density in the two oceans is not necessarily the same) is a few Sverdrups



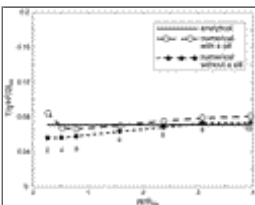
Click on thumbnail for full-sized image.

FIG. 6. (a) Observed depth variations of σ_θ in the deep South Pacific; dots indicate observed values [adapted from [Warren \(1977\)](#)]. (b) Qualitative curvature plots corresponding to (top) an upward motion and (bottom) a downward motion



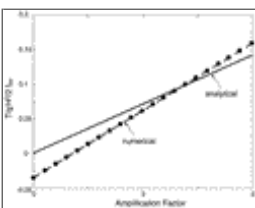
Click on thumbnail for full-sized image.

FIG. 7. The circulation pattern implied by the silicate distribution ($\mu\text{M kg}^{-1}$) [reproduced from [Craig et al. \(1981\)](#)]. The solid line constituting an upward motion to middepth represents the conventional interpretation of this distribution. The dashed line above represents the shallow MOC [implied by our quasi-island calculation and by [Hallberg and Toggweiler's \(1998\)](#) calculation]. It has been suggested ([Hallberg and Toggweiler 1998](#)) that a downward motion associated with an upper cell is necessary for the balance of heat (see text). This shallow-upper-cell idea is also consistent with the inverse calculations of [Wunsch et al. \(1983\)](#)




Click on thumbnail for full-sized image.

FIG. 8. A comparison of the analytically calculated meridional transport (solid horizontal line) and the numerically simulated values (dashed lines) for the diamond model with a varying gap width w . Solid dots (●) correspond to experiments without a sill and open circles (○) correspond to experiments with a sill occupying approximately 93% of the upper-layer undisturbed depth H (600 m). Numerals indicate number of grid points within the gap. Note that for gaps as wide as the (internal) Rossby radius the agreement between the analytics and the numerics is very good (but not excellent because of frictional processes that are absent from the analytics)



Click on thumbnail for full-sized image.

FIG. 9. A comparison of the analytically predicted transport (solid line) with the numerical transport for various wind patterns (see [Fig. 3a](#) , lower panel) acting on the diamond model without a sill (set C). The amplification factor is the ratio between the southern winds (ranging from 20 to 60 dynes cm^{-2}) and the northern winds. The ratio of the predicted northward transport (18 Sv) and $g' H^2/2f$ is approximately 0.1. As in the varying-gapwidth case, the agreement is good but not excellent (particularly for small transports). Discrepancies between the two are due to the presence of zonal boundary currents in the numerics. These zonal currents are balanced (in the numerics) by zonal friction, which is absent from the analytics. There is a very apparent systematic bias in the gradients of the lines but we unfortunately have been unable to determine its cause

* Additional affiliation: The Geophysical Fluid Dynamics Institute, The Florida State University, Tallahassee, Florida

Corresponding author address: Doron Nof, Dept. of Oceanography, The Florida State University, Tallahassee, FL 32306-4320. E-mail: nof@ocean.fsu.edu

